ARTICLE IN PRESS

Journal of Symbolic Computation ▮ (▮▮▮▮) ▮▮▮–▮▮▮

Contents lists available at ScienceDirect

Journal of Symbolic Computation

journal homepage: www.elsevier.com/locate/jsc

A tessellation for Fermat surfaces in $\mathbb{C}P^3$

Andrew J. Hanson [a,1], Ji-Ping Sha [b]

[a] Department of Computer Science, Indiana University, Bloomington, IN 47405, United States

[b] Department of Mathematics, Indiana University, Bloomington, IN 47405, United States

ARTICLE INFO

Article history:
Received 23 February 2008
Accepted 5 September 2008
Available online xxxx

Keywords:
Tessellation
Fermat surface
K3 surface
Complex projective space

ABSTRACT

For each positive integer n, we present a tessellation of $\mathbb{C}\mathbf{P}^2$ that can be lifted, through the branched covering, to a symmetric tessellation of the Fermat surface (a 4-manifold) of degree n in $\mathbb{C}\mathbf{P}^3$. The process is systematic and symbolically algebraic. Each four-cell in the tessellation is bounded by four pentahedrons, and each pentahedron has four triangular faces and one quadrilateral face. Graphically, one can produce the entire surface from one single four-cell using translations generated by permutations and phase multiplications of the homogeneous coordinates of $\mathbb{C}\mathbf{P}^3$. Note that the tessellation of the Fermat surface of degree 4, a K3 surface, has exactly 24 vertices.

In this paper, we present a systematic and explicit algorithm for tessellating the Fermat surfaces in $\mathbb{C}\mathbf{P}^3$. A Fermat surface in $\mathbb{C}\mathbf{P}^3$ is an algebraic surface (real 4-manifold) F_n defined by the equation

$$z_0^n + z_1^n + z_2^n + z_3^n = 0 \tag{1}$$

in the standard homogeneous coordinates $[z_0, z_1, z_2, z_3]$, where n is any positive integer. Note that F_4 in particular is a K3 surface (see, e.g., Griffiths and Harris (1978)).

The vertices of the tessellation we present are the n-th roots of unity in the six standard projective lines $\mathbb{C}\mathbf{P}^1$ in $\mathbb{C}\mathbf{P}^3$; they are the obvious vertices to start a construction of a natural tessellation for F_n. Our tessellation is invariant under the action of the isomorphism group of F_n induced by permutations and phase multiplications of the coordinates (here a phase multiplication means multiplying any of the coordinates by a number of the form $e^{i2k\pi/n}$), and the action is transitive on the set of 4-cells. The tessellation is built upon a similar triangulation for the corresponding algebraic curves in $\mathbb{C}\mathbf{P}^2$, and we believe the method can be generalized to the corresponding algebraic hypersurfaces in $\mathbb{C}\mathbf{P}^N$ for $N > 3$.

E-mail addresses: hansona@indiana.edu (A.J. Hanson), jsha@indiana.edu (J.-P. Sha).

[1] Tel.: +1 812 855 5855; fax: +1 812 855 4829.

0747-7171/$ – see front matter © 2008 Elsevier Ltd. All rights reserved.
doi:10.1016/j.jsc.2008.09.002

Please cite this article in press as: Hanson, A.J., Sha, J.-P., A tessellation for Fermat surfaces in $\mathbb{C}P^3$. Journal of Symbolic Computation (2008), doi:10.1016/j.jsc.2008.09.002

The tessellation is algorithmically programmable: for any given positive integer n, one first lists all the vertices; then all the edges, faces, 3-cells, and 4-cells can be produced symbolically from the list of vertices. One may then try, for example, to formulate the simplicial complex boundary map matrices explicitly and compute the homology of F_n and the intersection form in a more elementary way, although this may technically still be somewhat complicated.

Explicit representations of geometric objects such as manifolds are essential for any attempt to create visual images that help expose their features. While there exist many powerful mathematical methods that allow the calculation of the geometric and topological invariants of manifolds, human perception requires the construction of visual images. Thus, it can be useful to develop explicit descriptions of interesting families of manifolds that can be used in practice to create visual representations and pictures. Such explicit representations can also in principle be used to clarify the calculation and understanding of abstract invariants of the manifolds. Among the classes of geometric objects that have a long history of interest are the algebraic varieties defined by homogeneous polynomials in complex projective spaces. One such family, the algebraic curves in $\mathbb{C}\mathbf{P}^2$ (see, e.g., Hanson (1994)), has recently served the purpose of providing explicit images of cross-sections of Calabi–Yau spaces, and has been used to represent the hidden dimensions of string theory (Greene, 1999), for which very few other methods of producing images are available. While one might have guessed that the methods used for $\mathbb{C}\mathbf{P}^2$ could be extended trivially to $\mathbb{C}\mathbf{P}^3$ and other higher-dimensional projective spaces, the problem turns out to be fairly complex.

Let us now be more precise. We will show the following:

Theorem. *For any given positive integer n, there is a tessellation on F_n with $6n^3$ 4-cells. Each 4-cell is bounded by four pentahedrons. Each pentahedron is a pyramid with one quadrilateral face and four triangular faces. The tessellation is invariant under the action of the group Γ_n, where Γ_n consists of isomorphisms of F_n induced from permutations and phase multiplications of the homogeneous coordinates of $\mathbb{C}\mathbf{P}^3$. The group Γ_n acts transitively on the set of 4-cells of the tessellation.*

Altogether, the tessellation has $6n$ vertices, $12n^2$ edges, $8n^2 + 7n^3$ 2-cells ($3n^3$ quadrilaterals and $8n^2+4n^3$ triangles), $12n^3$ 3-cells (pyramids) and $6n^3$ 4-cells. It is known that the Euler characteristic of any smooth algebraic surface of degree n in $\mathbb{C}\mathbf{P}^3$ is $6n-4n^2+n^3$ (see, e.g., Griffiths and Harris (1978)). One handily verifies from our tessellation for F_n that this is equal to $6n-12n^2+(8n^2+7n^3)-12n^3+6n^3$, i.e., the alternating sum of the numbers of vertices, edges, 2-cells, 3-cells, and 4-cells.

Notice that the restriction to F_n of the natural projection $\mathbb{C}\mathbf{P}^3 \setminus \{[0,0,0,1]\} \to \mathbb{C}\mathbf{P}^2$, given by $[z_0, z_1, z_2, z_3] \mapsto [z_0, z_1, z_2]$, is a regular n-fold branched covering

$$\sigma : F_n \to \mathbb{C}\mathbf{P}^2 \tag{2}$$

which is branched over the algebraic curve in $\mathbb{C}\mathbf{P}^2$ defined by the equation

$$z_0^n + z_1^n + z_2^n = 0. \tag{3}$$

The tessellation of F_n we present is a lift from σ of a tessellation of $\mathbb{C}\mathbf{P}^2$, which is an extension of a tessellation (triangulation) of the algebraic curve (3). This approach greatly reduces the difficulty caused by the topological complexity of F_n, as the geometry and topology of $\mathbb{C}\mathbf{P}^2$ are much easier to handle and visualize. We also implicitly assume that $\mathbb{C}\mathbf{P}^2$ is equipped with the standard Fubini–Study Riemannian metric. In particular, every projective line $\mathbb{C}\mathbf{P}^1$ in $\mathbb{C}\mathbf{P}^2$ is totally geodesic, and, with the induced metric, is a round 2-sphere; the real projective planes are also totally geodesic and have induced metric of constant curvature.

1. Tessellation of the algebraic curve

Denote by S_n the algebraic curve in $\mathbb{C}\mathbf{P}^2$ defined by (3). In this section, we will tessellate (i.e., triangulate) S_n in a specific way so that we can extend the tessellation to the $\mathbb{C}\mathbf{P}^2$ in the next section. The tessellation is, in fact, a lifting of a natural tessellation on $\mathbb{C}\mathbf{P}^1$ for the given n.

The projection $\mathbb{C}\mathbf{P}^2 \setminus \{[0,0,1]\} \to \mathbb{C}\mathbf{P}^1$, given by $[z_0, z_1, z_2] \mapsto [z_0, z_1]$ induces a regular n-fold branched covering from S_n to the $\mathbb{C}\mathbf{P}^1$ branched at n points,

$$p_k := [1, e^{i(\pi+2k\pi)/n}], \quad k = 0, \ldots, n-1. \tag{4}$$

Please cite this article in press as: Hanson, A.J., Sha, J.-P., A tessellation for Fermat surfaces in $\mathbb{C}P^3$. Journal of Symbolic Computation (2008), doi:10.1016/j.jsc.2008.09.002

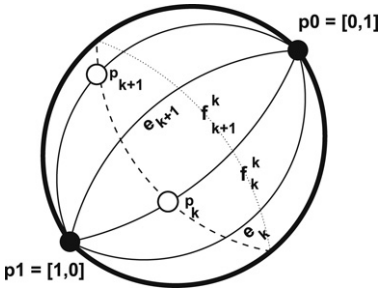

Fig. 1.

We first formulate a tessellation for the $\mathbb{C}\mathbf{P}^1$, which has $n+2$ vertices, $3n$ edges and $2n$ triangles: Let

$$p0 := [0,\ 1], \quad p1 := [1,\ 0] \tag{5}$$

and join them by the following n paths,

$$e_k(t) := [\cos t,\ \sin t\, \mathrm{e}^{\mathrm{i}2k\pi/n}], \quad 0 \le t \le \frac{\pi}{2},\ k = 0, \ldots, n-1. \tag{6}$$

Then the $2n$ triangles of the tessellation are

$$f_k^k, \quad f_{k+1}^k, \quad k = 0, \ldots, n-1 \,(\mathrm{mod}\, n), \tag{7}$$

where each of f_k^k, f_{k+1}^k is the triangle with vertices $p0$, $p1$, p_k, the edge e_k, or e_{k+1}, respectively, and the other two edges given by the minimizing geodesics joining p_k and $p0$, $p1$ (see Fig. 1).

Lifting this triangulation through the branched covering, we then get a triangulation for S_n. There are $3n$ vertices,

$$p0_k := [0,\ 1,\ \mathrm{e}^{\mathrm{i}(\pi+2k\pi)/n}], \qquad p1_k := [\mathrm{e}^{\mathrm{i}(\pi+2k\pi)/n},\ 0,\ 1], \qquad p2_k := [1,\ \mathrm{e}^{\mathrm{i}(\pi+2k\pi)/n},\ 0],$$

for $k = 0, \ldots, n-1 \,(\mathrm{mod}\, n)$, and $2n^2$ triangles. It is not hard to see that these triangles, as lifts of f_k^k, f_{k+1}^k and expressed in terms of their vertices, are $\triangle p0_{j-k} p1_{-j-1} p2_k$, $\triangle p0_{j-(k+1)} p1_{-j-1} p2_k$, respectively. We denote them by the following:

$$b_{j-k,-j-1,k}, \qquad b_{j-(k+1),-j-1,k}, \quad j, k = 0, \ldots, n-1 \,(\mathrm{mod}\, n). \tag{8}$$

To be more clear, we verify the indices in (8) by showing the edges of these triangles explicitly.

The three edges of $b_{j-(k+1),-j-1,k}$, in the order $p2_k - p0_{j-(k+1)} - p1_{-j-1} - p2_k$, can be described as follows: notice that the first two coordinates give the edges of f_{k+1}^k, in the order $p_k - p0 \overset{e_{k+1}}{-} p1 - p_k$, and the factor $\mathrm{e}^{\mathrm{i}2j\pi/n}$ on the third coordinate specifies a certain branch to which f_{k+1}^k is lifted.

$$\begin{aligned}
&[\cos t,\ \sin t\, \mathrm{e}^{\mathrm{i}(2k+1)\pi/n},\ \mathrm{e}^{\mathrm{i}2j\pi/n}(-\cos^n t + \sin^n t)^{1/n}], \quad \pi/4 \le t \le \pi/2;\\
&[\sin t,\ \cos t\, \mathrm{e}^{\mathrm{i}2(k+1)\pi/n},\ \mathrm{e}^{\mathrm{i}2j\pi/n}(-\sin^n t - \cos^n t)^{1/n}], \quad 0 \le t \le \pi/2;\\
&[\cos t,\ \sin t\, \mathrm{e}^{\mathrm{i}(2k+1)\pi/n},\ \mathrm{e}^{\mathrm{i}2j\pi/n}(-\cos^n t + \sin^n t)^{1/n}], \quad 0 \le t \le \pi/4.
\end{aligned} \tag{9}$$

Similarly, the three edges of $b_{j-k,-j-1,k}$, in the order $p2_k - p1_{-j-1} - p0_{j-k} - p2_k$, as lifts of those of f_k^k, in the order $p_k - p1 \overset{e_k}{-} p0 - p_k$, are

$$\begin{aligned}
&[\sin t,\ \cos t\, \mathrm{e}^{\mathrm{i}(2k+1)\pi/n},\ \mathrm{e}^{\mathrm{i}2j\pi/n}(-\sin^n t + \cos^n t)^{1/n}], \quad \pi/4 \le t \le \pi/2;\\
&[\cos t,\ \sin t\, \mathrm{e}^{\mathrm{i}2k\pi/n},\ \mathrm{e}^{\mathrm{i}2j\pi/n}(-\cos^n t - \sin^n t)^{1/n}], \quad 0 \le t \le \pi/2;\\
&[\sin t,\ \cos t\, \mathrm{e}^{\mathrm{i}(2k+1)\pi/n},\ \mathrm{e}^{\mathrm{i}2(j+1)\pi/n}(-\sin^n t + \cos^n t)^{1/n}], \quad 0 \le t \le \pi/4.
\end{aligned} \tag{10}$$

Notice that there is a branch shift on the lift of $p0 - p_k$ (see Fig. 2).

Please cite this article in press as: Hanson, A.J., Sha, J.-P., A tessellation for Fermat surfaces in $\mathbb{C}\mathrm{P}^3$. Journal of Symbolic Computation (2008), doi:10.1016/j.jsc.2008.09.002

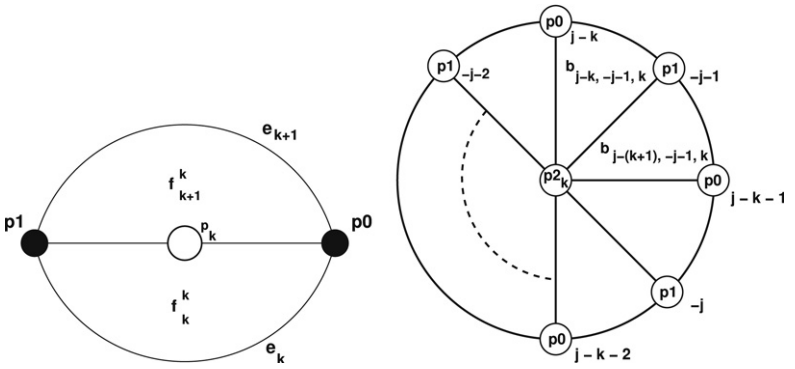

Fig. 2.

From (9) and (10) one then gets the vertices for the corresponding triangles easily. We note that any one of the indices for b in (8) is determined by the other two according to the rule that the sum of the three indices is equal to -1 or -2, respectively.

The tessellation is invariant under the isomorphisms of S_n induced from permutations and phase multiplications of the homogeneous coordinates of $\mathbb{C}\mathbf{P}^2$. To see this, first notice that the tessellation on $\mathbb{C}\mathbf{P}^1$ is obviously invariant under the corresponding isomorphisms: the vertices are invariant and the edges are all geodesics while the isomorphisms are isometries. The tessellation is also obviously invariant under the phase multiplication of z_2 because the latter is just a deck transformation of the branched covering. Therefore it suffices only to verify the invariance under interchanging the coordinates z_1 and z_2.

After interchanging z_1 and z_2, the three paths in (10) become

$$
\begin{aligned}
&[\sin t, \mathrm{e}^{\mathrm{i}2j\pi/n}(-\sin^n t + \cos^n t)^{1/n}, \cos t \mathrm{e}^{\mathrm{i}(2k+1)\pi/n}], \quad \pi/4 \le t \le \pi/2;\\
&[\cos t, \mathrm{e}^{\mathrm{i}2j\pi/n}(-\cos^n t - \sin^n t)^{1/n}, \sin t \mathrm{e}^{\mathrm{i}2k\pi/n}], \quad 0 \le t \le \pi/2;\\
&[\sin t, \mathrm{e}^{\mathrm{i}2(j+1)\pi/n}(-\sin^n t + \cos^n t)^{1/n}, \cos t \mathrm{e}^{\mathrm{i}(2k+1)\pi/n}], \quad 0 \le t \le \pi/4.
\end{aligned}
$$

They are the same as

$$
\begin{aligned}
&[\sin t, \mathrm{e}^{\mathrm{i}(2j+1)\pi/n}(\sin^n t - \cos^n t)^{1/n}, \cos t \mathrm{e}^{\mathrm{i}(2k+1)\pi/n}], \quad \pi/4 \le t \le \pi/2;\\
&[\cos t, \mathrm{e}^{\mathrm{i}(2j+1)\pi/n}(\cos^n t + \sin^n t)^{1/n}, \sin t \mathrm{e}^{\mathrm{i}2k\pi/n}], \quad 0 \le t \le \pi/2;\\
&[\sin t, \mathrm{e}^{\mathrm{i}2(j+1)\pi/n}(-\sin^n t + \cos^n t)^{1/n}, \cos t \mathrm{e}^{\mathrm{i}(2k+1)\pi/n}], \quad 0 \le t \le \pi/4;
\end{aligned}
$$

or

$$
\begin{aligned}
&[\cos t, \mathrm{e}^{\mathrm{i}(2j+1)\pi/n}(\cos^n t + \sin^n t)^{1/n}, \mathrm{e}^{\mathrm{i}2k\pi/n}(\sin^n t)^{1/n}], \quad 0 \le t \le \pi/2;\\
&[\sin t, \mathrm{e}^{\mathrm{i}2(j+1)\pi/n}(-\sin^n t + \cos^n t)^{1/n}, \mathrm{e}^{\mathrm{i}2k\pi/n}(-\cos^n t)^{1/n}], \quad 0 \le t \le \pi/4.\\
&[\sin t, \mathrm{e}^{\mathrm{i}(2j+1)\pi/n}(\sin^n t - \cos^n t)^{1/n}, \mathrm{e}^{\mathrm{i}2k\pi/n}(-\cos^n t)^{1/n}], \quad \pi/4 \le t \le \pi/2;
\end{aligned}
$$

which are the edges of $b_{k-(j+1),-k-1,j}$, a lift of f^j_{j+1}. Similarly, interchanging z_1 and z_2 transforms $b_{j-(k+1),-j-1,k}$ to $b_{k-j,-k-1,j}$.

It is easy to see that the transformation under these isomorphisms is transitive on triangles. As the number of the isomorphisms is $6n^2$, the order of isotropy of each triangle is 3, consisting of the cyclic edge permutations. Therefore, the transformation is also transitive on the edges, and obviously on the vertices as well.

We finally point out that the case $n = 1$ is somewhat peculiar: the two triangles share the same three edges. Therefore extra care in labeling, e.g, specifying the orientation, is needed.

Please cite this article in press as: Hanson, A.J., Sha, J.-P., A tessellation for Fermat surfaces in $\mathbb{C}\mathrm{P}^3$. Journal of Symbolic Computation (2008), doi:10.1016/j.jsc.2008.09.002

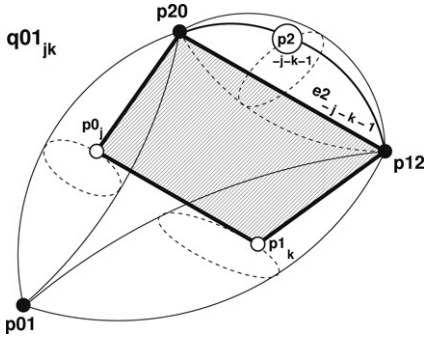

Fig. 3.

2. Extended tessellation on $\mathbb{C}\mathbf{P}^2$

In this section, we extend the tessellation of S_n described in Section 1 to a tessellation of the $\mathbb{C}\mathbf{P}^2$. Then, by lifting, that will automatically produce a tessellation of F_n.

Denote the projective line $z_j = 0$ by L_j, for $j = 0, 1, 2$, and let

$$p01 := [0, 0, 1], \quad p12 := [1, 0, 0], \quad p20 := [0, 1, 0]. \tag{11}$$

We start by specifying the other 2-cells for the tessellation.

Note that on L_0, the points $p01$, $p20$ and the intersections with the S_n, namely $p0_k$, $k = 0, \ldots, n-1$, form the exact same configuration as (5) and (4) on $\mathbb{C}\mathbf{P}^1$ described in Section 1. We then add the corresponding $2n$ triangles (7); similarly for the lines L_1 and L_2. Therefore altogether there are $6n$ new triangles, which we label as follows:

$$ff^{\,k}_{\,k}, \quad ff^{\,k}_{\,k+1}, \quad j = 0, 1, 2 \quad \text{and} \quad k = 0, \ldots, n-1 \,(\text{mod } n). \tag{12}$$

Label the edges corresponding to those in (6) by $ej_{\,k}$. Notice that, for example, as a path, $e1_{\,k}(t) = [\sin t\, e^{i2k\pi/n}, 0, \cos t]$.

In the next group, each triangle is formed by minimizing geodesics joining one of the vertices $p01, p12, p20$ to the edge on S_n, e.g., $p2_j - p0_k$ in the case of $p20$. We denote these $3n^2$ triangles as follows:

$$h01_{jk}, \quad h12_{jk}, \quad h20_{jk}, \quad j, k = 0, \ldots, n-1 \,(\text{mod } n). \tag{13}$$

We remark that all the triangles in (13) are totally geodesic; one sees, e.g., from (9) that they are pieces of real projective planes. In fact, all the new 2-cells we add will be totally geodesic.

There is one more group of n^2 triangles that all have the same three vertices $p01, p12, p20$. For clarity, we write down the following explicit parameterizations for them:

$$g_{jk}(s, t) = [\cos s, \sin s \cos t e^{i2j\pi/n}, \sin s \sin t e^{i2k\pi/n}], \quad 0 \le s, t \le \pi/2.$$

The three edges of g_{jk} are $e0_{\,k-j}$, $e1_{\,-k}$, $e2_{\,j}$. For convenience, we will denote g_{jk} by

$$g_{k-j,-k,j}, \quad j, k = 0, \ldots, n-1 \,(\text{mod } n), \tag{14}$$

noticing again that any one of the indices of g is determined by the other two according to the rule that the sum of the three indices is equal to 0.

The next set of 2-cells is a set of $3n^2$ quadrilaterals. They are in one-to-one correspondence with the edges in S_n; each edge is one side of exactly one quadrilateral. For example, the edge $p0_j - p1_k$ is a side of the quadrilateral having $e2_{-j-k-1}$ as the opposite side of $p0_j - p1_k$; recall that $e2_{-j-k-1}$ is in L_2 between the two vertices $p2_{-j-k-2}$ and $p2_{-j-k-1}$, which are, respectively, the vertices of the two triangles in S_n having $p0_j - p1_k$ as a common side. See Fig. 3.

The quadrilateral is formed by minimizing geodesics joining the points on $e2_{-j-k-1}$ to the distance-proportional points on $p0_j - p1_k$. In particular, the two edges in L_0, L_1 joining $p20$, $p12$ and $p0_j$, $p1_k$,

Please cite this article in press as: Hanson, A.J., Sha, J.-P., A tessellation for Fermat surfaces in $\mathbb{C}\mathrm{P}^3$. Journal of Symbolic Computation (2008), doi:10.1016/j.jsc.2008.09.002

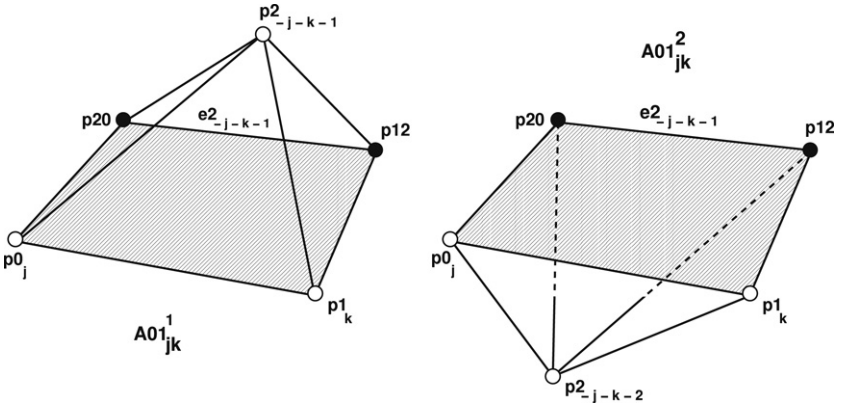

Fig. 4.

respectively, are the other two sides of the quadrilateral. We denote this quadrilateral by $q01_{jk}$ and the set of quadrilaterals is

$$q01_{jk}, \quad q12_{jk}, \quad q20_{jk}, \quad j,k=0,\ldots,n-1\,(\mathrm{mod}\,n). \tag{15}$$

This concludes our construction of the 2-cells. The only new vertices added are then those in (11) and the only new edges are those in the L_j's.

We now proceed to describe the 3-cells. It should be pointed out that, up to now, the cells constructed can be easily verified to be embedded in $\mathbb{C}\mathbf{P}^2$, and there is no intersection among them in the interior of any cell. As the dimension of the cell becomes higher, this becomes less clear *a priori*. We will show later that the cells do form a tessellation for the $\mathbb{C}\mathbf{P}^2$.

The 3-cells are divided into two groups. Each of them is in two-to-one correspondence with the set of edges in S_n, or the set of quadrilaterals. In fact, every quadrilateral is a face of exactly two 3-cells in each group.

In the first group, the two 3-cells corresponding to, say, the edge $p0_j$–$p1_k$ are formed by interpolating between distance-proportional points on $b_{j,k,-j-k-1}$, $b_{j,k,-j-k-2}$ and $f2^{-j-k-1}_{-j-k-1}, f2^{-j-k-2}_{-j-k-1}$, respectively, by minimizing geodesics (see Fig. 4).

Clearly, the 3-cell is a pyramid. Besides the quadrilateral face $q01_{jk}$, the other four faces are the triangles

$$\{b_{j,k,-j-k-1}, \quad h12_{k,-j-k-1}, \quad h20_{-j-k-1,j}, \quad f2^{-j-k-1}_{-j-k-1}\},$$

or

$$\{b_{j,k,-j-k-2}, \quad h12_{k,-j-k-2}, \quad h20_{-j-k-2,j}, \quad f2^{-j-k-1}_{-j-k-2}\},$$

respectively. Denote these pyramids by $A01^1_{jk}$, $A01^2_{jk}$, respectively. We can now list all the $6n^2$ 3-cells in the first group:

$$\begin{aligned} &A01^1_{jk}, \quad A01^2_{jk},\\ &A12^1_{jk}, \quad A12^2_{jk}, \quad j,k=0,\ldots,n-1\,(\mathrm{mod}\,n).\\ &A20^1_{jk}, \quad A20^2_{jk}. \end{aligned} \tag{16}$$

In the second group of 3-cells, the two corresponding to, say again, $p0_j$–$p1_k$ are formed by minimizing geodesic interpolation between $h01_{jk}$ and $g_{j,k+1,-j-k-1}$, $g_{j+1,k,-j-k-1}$, respectively (see Fig. 5).

Clearly, each 3-cell is also a pyramid. Besides the quadrilateral face $q01_{jk}$, the other four faces are the triangles

$$\{g_{j,k+1,-j-k-1}, \quad f0^j_j, \quad f1^k_{k+1}, \quad h01_{jk}\},$$

Please cite this article in press as: Hanson, A.J., Sha, J.-P., A tessellation for Fermat surfaces in $\mathbb{C}\mathrm{P}^3$. Journal of Symbolic Computation (2008), doi:10.1016/j.jsc.2008.09.002

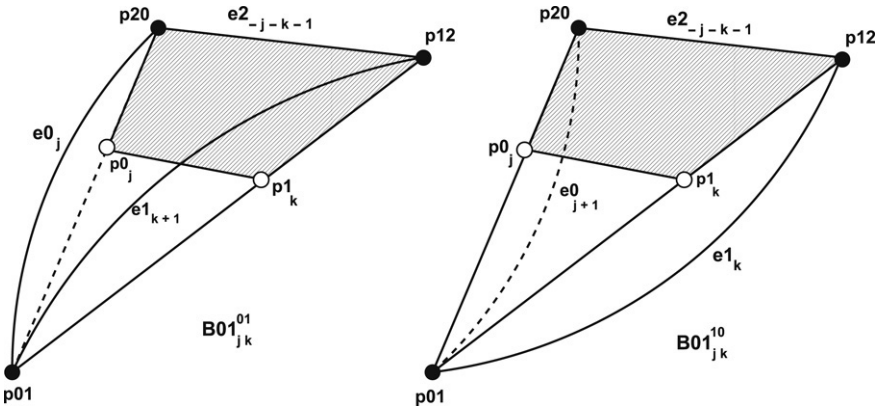

Fig. 5.

or

$$\{g_{j+1,k,-j-k-1},\quad f0^{j}_{j+1},\quad f1^{k}_{k},\quad h01_{jk}\},$$

respectively. Notice that, unlike the first group, whose two pyramids share only the quadrilateral face, these two pyramids share both the quadrilateral face $q01_{jk}$ and the triangular face $h01_{jk}$. Denote these pyramids by $B01^{01}_{jk}$, $B01^{10}_{jk}$, respectively. The list of all the $6n^2$ 3-cells in the second group then is:

$$\begin{aligned}
&B01^{01}_{jk},\quad B01^{10}_{jk},\\
&B12^{01}_{jk},\quad B12^{10}_{jk},\quad j,k=0,\ldots,n-1\,(\mathrm{mod}\,n).\\
&B20^{01}_{jk},\quad B20^{10}_{jk}.
\end{aligned}\tag{17}$$

We are now ready to tessellate the $\mathbb{C}\mathbf{P}^2$ by 4-cells. Each 4-cell is bounded by four pyramids, two from each of the groups (16) and (17); in fact, two from one determine the two from the other. Since every 3-cell should be the face of exactly two 4-cells, it follows that there are in all $6n^2$ 4-cells. We illustrate one of them as follows.

Start with $A01^{1}_{jk}$ in (16). The other pyramid from (16) is either $A12^{1}_{k,-j-k-1}$ or $A20^{1}_{-j-k-1,j}$, as these are the only other two pyramids in (16) sharing the triangular face $b_{j,k,-j-k-1}$ with $A01^{1}_{jk}$. If, say, we pick $A12^{1}_{k,-j-k-1}$, then it is easy to see that the two pyramids from (17) must be $B01^{01}_{jk}$ and $B12^{10}_{k,-j-k-1}$, in order to have the quadrilateral faces $q01_{jk}$ and $q12_{k,-j-k-1}$ shared, and for the two to have the triangular face from (14) in common. Therefore this 4-cell is bounded by the following four pyramids:

$$\{A01^{1}_{jk},\quad A12^{1}_{k,-j-k-1},\quad B01^{01}_{jk},\quad B12^{10}_{k,-j-k-1}\}.\tag{18}$$

As illustrated in Fig. 6, the pyramids in (18) indeed form a tessellation for a 3-sphere, at least combinatorially.

From the above, it is easy now to list all the 4-cells in terms of their boundary pyramids:

$$\begin{aligned}
&\{A01^{1}_{jk},\ A12^{1}_{k,-j-k-1},\ B01^{01}_{jk},\ B12^{10}_{k,-j-k-1}\},\\
&\{A01^{2}_{jk},\ A12^{2}_{k,-j-k-2},\ B01^{10}_{jk},\ B12^{01}_{k,-j-k-2}\},\\
&\{A12^{1}_{jk},\ A20^{1}_{k,-j-k-1},\ B12^{01}_{jk},\ B20^{10}_{k,-j-k-1}\},\\
&\{A12^{2}_{jk},\ A20^{2}_{k,-j-k-2},\ B12^{10}_{jk},\ B20^{01}_{k,-j-k-2}\},\\
&\{A20^{1}_{jk},\ A01^{1}_{k,-j-k-1},\ B20^{01}_{jk},\ B01^{10}_{k,-j-k-1}\},\\
&\{A20^{2}_{jk},\ A01^{2}_{k,-j-k-2},\ B20^{10}_{jk},\ B01^{01}_{k,-j-k-2}\},
\end{aligned}\tag{19}$$

Please cite this article in press as: Hanson, A.J., Sha, J.-P., A tessellation for Fermat surfaces in $\mathbb{C}\mathrm{P}^3$. Journal of Symbolic Computation (2008), doi:10.1016/j.jsc.2008.09.002

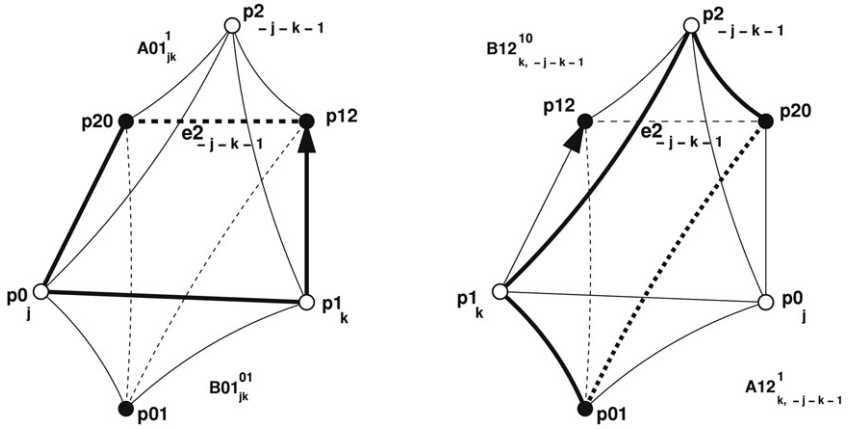

Fig. 6.

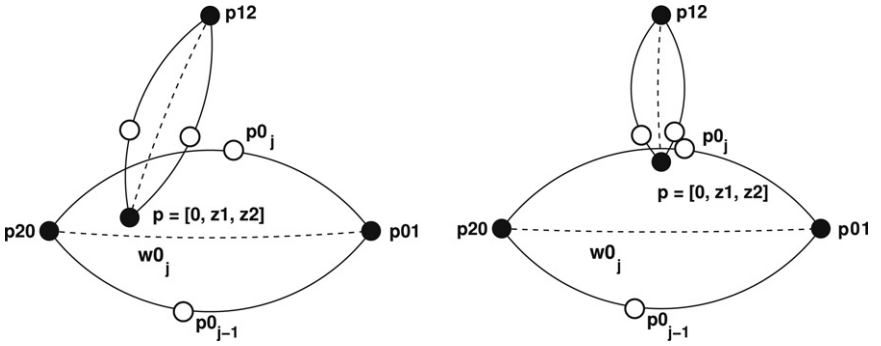

Fig. 7.

for $j, k = 0, \ldots, n-1 \pmod n$. Combinatorially, these $6n^2$ 4-cells together form a simplicial 4-manifold. Combining this with the numbers of vertices, edges, 2-cells, and 3-cells we have obtained before, we find its Euler characteristic number to be

$$(3n+3) - (3n^2+9n) + (2n^2+6n+3n^2+n^2+3n^2) - 12n^2 + 6n^2 = 3,$$

which is the Euler characteristic of $\mathbb{C}\mathbf{P}^2$. However, as we pointed out earlier, to show this is really a tessellation of the $\mathbb{C}\mathbf{P}^2$, one needs to verify that all the 4-cells are embedded and that there is no intersection among them at any of their interior points. We now confirm this.

For any fixed point $p = [0, z_1, z_2] \in L_0$ let $L_{0,p}$ be the projective line joining $p12$ and p. Then $\mathbb{C}\mathbf{P}^2 = \bigcup_{p\in L_0} L_{0,p}$; the union is disjoint except that all the $L_{0,p}$'s intersect at the single point $p12$. It is easy to verify, (i) if $p \notin S_n$, then $L_{0,p}$ intersects S_n at exactly n different points in a similar position to those in (4) on $\mathbb{C}\mathbf{P}^1$, and (ii) if $p \in S_n$ then p is the only intersection of $L_{0,p}$ and S_n.

For $p \notin S_n$, we triangulate $L_{0,p}$ similarly to $\mathbb{C}\mathbf{P}^1$, using the points $p12$, p (corresponding to the vertices in (5)), and the n intersections with S_n (see Fig. 7).

Notice that for $p \in S_n$, although we do not have the triangulation, there are n well defined paths from $p12$ to p that are obtained as limits of the paths on $L_{0,q}$, for q near $p \in S_n$ on L_0, corresponding to the edges joining $p0$ in (5) and the p_k's in (4). Also notice, in particular, that $L_{0,p01} = L_1$ and $L_{0,p20} = L_2$.

Let

$$wl_k = fl_k^{k-1} \cup fl_k^k, \quad l = 0, 1, 2;\ k = 0, \ldots, n-1 \pmod n.$$

For given j and k, as p varies on $w0_j$, it is easy to see that we get a continuous family of regions $w1_{k,p}$ in $L_{0,p}$ with $w1_{k,p01} = w1_k$. The union of this family of regions then clearly forms an embedded 4-cell

Please cite this article in press as: Hanson, A.J., Sha, J.-P., A tessellation for Fermat surfaces in $\mathbb{C}P^3$. Journal of Symbolic Computation (2008), doi:10.1016/j.jsc.2008.09.002

in the $\mathbb{C}\mathbf{P}^2$, which we will denote by $W_{j,k,-j-k}$. It is also clear that $\mathbb{C}\mathbf{P}^2 = \bigcup_{j,k} W_{j,k,-j-k}$ and there is no intersection between different $W_{j,k,-j-k}$'s at any of their interior points.

For clarity and later convenience, we write down the following explicit parametrization for $W_{j,k,-j-k}$:

$$[\cos s\, e^{i\beta}, \cos r \sin s, \sin r \sin s\, e^{i\alpha}] \tag{20}$$

with $0 \le r, s \le \pi/2$, $(2j-1)\pi/n \le \alpha \le (2j+1)\pi/n$ and, if we denote $\arg(-\cos^n r - \sin^n r\, e^{in\alpha})$ by $a(r,\alpha)$ with $0 \le a(r,\alpha) \le 2\pi$, then

$$\frac{a(r,\alpha)+2(j+k-1)\pi}{n} \le \beta \le \frac{a(r,\alpha)+2(j+k)\pi}{n}.$$

We see in particular that $w1_{k,p20} = w2_{-j-k}$. See Fig. 8.

From (20), it follows that, in a way similar to the above, $W_{j,k,-j-k}$ can also be described as a union of $w2_{-j-k,p}$ over $p \in w1_k$, or a union of $w0_{j,p}$ over $p \in w2_{-j-k}$. Therefore the boundary of $W_{j,k,-j-k}$ is tessellated by twelve 3-cells; each of them is the union of one of the two lower half boundary edges of a w-region over one of the two triangles in the corresponding base region. It is easy to see that these 3-cells are in fact exactly the following twelve pyramids in (16):

$$\begin{array}{llll} A12^1_{k-1,-j-k}, & A12^2_{k-1,-j-k}, & A12^1_{k,-j-k-1}, & A12^2_{k,-j-k-1}, \\ A20^1_{-j-k-1,j}, & A20^2_{-j-k-1,j}, & A20^1_{-j-k,j-1}, & A20^2_{-j-k,j-1}, \\ A01^1_{j-1,k}, & A01^2_{j-1,k}, & A01^1_{j,k-1}, & A01^2_{j,k-1}. \end{array} \tag{21}$$

It is also easy to see there are six 3-cells contained inside $W_{j,k,-j-k}$; each of them is the union of one of the two triangles in a w-region over the middle edge of the corresponding base region. These 3-cells are the following six pyramids in (17):

$$\begin{array}{ll} B12^{10}_{k-1,-j-k}, & B12^{01}_{k,-j-k-1} \\ B20^{10}_{-j-k-1,j}, & B20^{01}_{-j-k,j-1}, \\ B01^{10}_{j-1,k}, & B01^{01}_{j,k-1}. \end{array} \tag{22}$$

These 3-cells divide $W_{j,k,-j-k}$ into six 4-cells; they are the following six in (19):

$$\begin{array}{llll} \{A01^1_{j,k-1}, & A12^1_{k-1,-j-k}, & B01^{01}_{j,k-1}, & B12^{10}_{k-1,-j-k}\}, \\ \{A12^2_{k-1,-j-k}, & A20^2_{-j-k,j-1}, & B12^{10}_{k-1,-j-k}, & B20^{01}_{-j-k,j-1}\}, \\ \{A20^1_{-j-k,j-1}, & A01^1_{j-1,k}, & B20^{01}_{-j-k,j-1}, & B01^{10}_{j-1,k}\}, \\ \{A01^2_{j-1,k}, & A12^2_{k,-j-k-1}, & B01^{10}_{j-1,k}, & B12^{01}_{k,-j-k-1}\}, \\ \{A12^1_{k,-j-k-1}, & A20^1_{-j-k-1,j}, & B12^{01}_{k,-j-k-1}, & B20^{10}_{-j-k-1,j}\}, \\ \{A20^2_{-j-k-1,j}, & A01^2_{j,k-1}, & B20^{10}_{-j-k-1,j}, & B01^{01}_{j,k-1}\}. \end{array} \tag{23}$$

The structure of (21)–(23) together can be illustrated by the diagram in Fig. 9.

Now it is clear that the $\mathbb{C}\mathbf{P}^2$ is well tessellated.

Remark. If all we need is a tessellation of the $\mathbb{C}\mathbf{P}^2$ (and hence F_n), then the triangles in (14) and the 3-cells in (17) are not needed. The pyramids in (16) are paired into $3n^2$ octahedrons, and the 4-cells of the tessellation are precisely the n^2 $W_{j,k,-j-k}$'s. However, when this tessellation is lifted to F_n, it is not Γ_n-invariant.

3. Tessellation of F_n

Through the n-fold regular branched covering (2), the tessellation of $\mathbb{C}\mathbf{P}^2$ in Section 2 now lifts to a well defined tessellation for the F_n. The numbers of vertices, edges, 2-cells, 3-cells and 4-cells are as indicated in the introduction. In this section, we examine this tessellation more closely and show that it is Γ_n-invariant. Recall that Γ_n is the group of the isomorphisms of F_n induced from permuting and/or phase multiplying the homogeneous coordinates of $\mathbb{C}\mathbf{P}^3$.

Please cite this article in press as: Hanson, A.J., Sha, J.-P., A tessellation for Fermat surfaces in $\mathbb{C}P^3$. Journal of Symbolic Computation (2008), doi:10.1016/j.jsc.2008.09.002

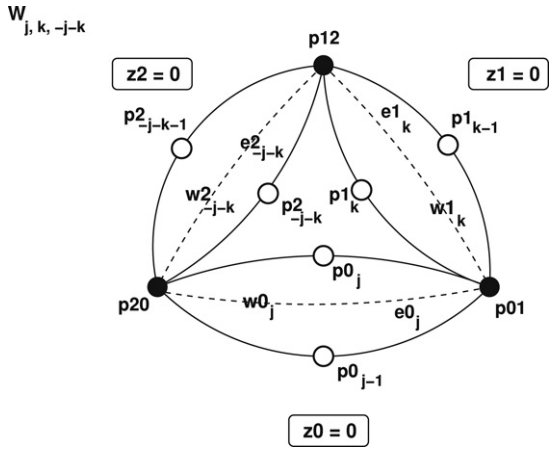

Fig. 8.

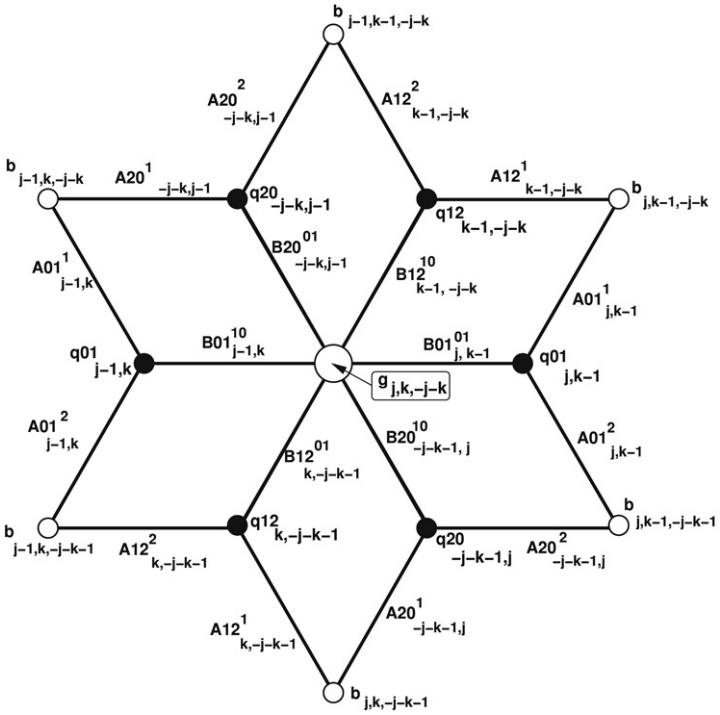

Fig. 9.

The intersection of F_n with each of the projective planes $z_k = 0$, $k = 0, 1, 2, 3$, is the S_n in that plane, triangulated as described in Section 1. The tessellation of the F_n is an extension of the triangulations on these four S_n's. In fact, the four S_n's contain all the vertices, edges, and triangles lifted from those in (8) and (12). The other $4n^3$ triangles are lifted from (13) and (14) and are characterized by the fact that for each of them, the three edges lie on three distinct S_n's. Notice then that for any three S_n's of the four, any three different pairwise intersections are vertices of a unique triangle lifted from (13) or (14).

Please cite this article in press as: Hanson, A.J., Sha, J.-P., A tessellation for Fermat surfaces in $\mathbb{CP}^3$. Journal of Symbolic Computation (2008), doi:10.1016/j.jsc.2008.09.002

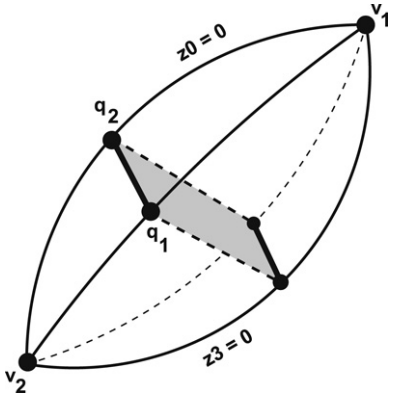

Fig. 10.

The formation of the quadrilaterals can be described as follows. Start with any edge on one of the four S_n's, say, the one in the projective plane $z_0 = 0$; its two end points, denoted by q_1 and q_2, must then also lie in two other distinct projective planes, say, $z_1 = 0$ and $z_2 = 0$, respectively. Then there are n distinct edges on $z_2 = 0$ joining q_2 and the n distinct intersections of the projective planes $z_2 = 0$ and $z_3 = 0$. Any one of these edges plus $\overline{q_1 q_2}$, the edge we started with, form two adjacent sides of a unique quadrilateral. Hence one sees that there are in all $3n^3$ quadrilaterals.

For two opposite sides, say, lying in the projective planes $z_0 = 0$ and $z_3 = 0$, respectively, of a given quadrilateral, as in the example above, there are exactly two vertices, v_1, v_2, in the intersection of $z_0 = 0$ and $z_3 = 0$ that are the opposite vertices of the given edges in triangles lying in $z_0 = 0$ and $z_3 = 0$, respectively (see Fig. 10). Each of these two vertices forms a pyramid with the quadrilateral. Notice that if one starts with the other pair of opposite sides of the quadrilateral, the two vertices will be different. One sees that there are in all $12n^3$ pyramids.

Finally, every 4-cell is bounded by four pyramids, and each pyramid is shared by two 4-cells, thus there are $6n^3$ 4-cells.

From the description above, one can see that if, instead of (2) which is induced from the projection $[z_0, z_1, z_2, z_3] \mapsto [z_0, z_1, z_2]$, we use the branched covering induced from, say, $[z_0, z_1, z_2, z_3] \mapsto [z_1, z_2, z_3]$, the lifted tessellation will be the same. This, combined with the invariance for S_n demonstrated in Section 1, shows that the tessellation of the F_n is Γ_n-invariant and the action of Γ_n is transitive on the set of 4-cells.

The list of all the vertices in the tessellation is:

$$p01_k := [0, 0, 1, e^{i(\pi+2k\pi)/n}], \quad p02_k := [0, 1, 0, e^{i(\pi+2k\pi)/n}],$$
$$p03_k := [0, 1, e^{i(\pi+2k\pi)/n}, 0], \quad p12_k := [1, 0, 0, e^{i(\pi+2k\pi)/n}],$$
$$p13_k := [1, 0, e^{i(\pi+2k\pi)/n}, 0], \quad p23_k := [1, e^{i(\pi+2k\pi)/n}, 0, 0],$$

for $k = 0, \ldots, n-1$.

One can then list the edges, 2-cells, 3-cells, and 4-cells in terms of the vertices. We now write down a few lists of edges and 2-cells for illustration (see Fig. 11).

Every edge lies on one of the four $\mathbb{C}\mathbf{P}^2$'s defined by $z_k = 0$. For example, the $3n^2$ edges lying on $z_0 = 0$ are:

$$\{p01_i,\ p02_j\}, \quad \{p01_i,\ p03_j\}, \quad \{p02_i,\ p03_j\},$$

$i, j = 0, \ldots, n-1$.

The 2-cells are divided into three groups: triangles each of which lies on one of the four $\mathbb{C}\mathbf{P}^2$'s defined by $z_k = 0$; triangles each of which has three sides on three different $\mathbb{C}\mathbf{P}^2$'s; rectangles.

For example, the $2n^2$ triangles lying on $z_0 = 0$ are:

$$\{p01_i,\ p02_j,\ p03_k\}, \quad i - j + k = 0 \text{ or } -1 \pmod n.$$

Please cite this article in press as: Hanson, A.J., Sha, J.-P., A tessellation for Fermat surfaces in $\mathbb{C}P^3$. Journal of Symbolic Computation (2008), doi:10.1016/j.jsc.2008.09.002

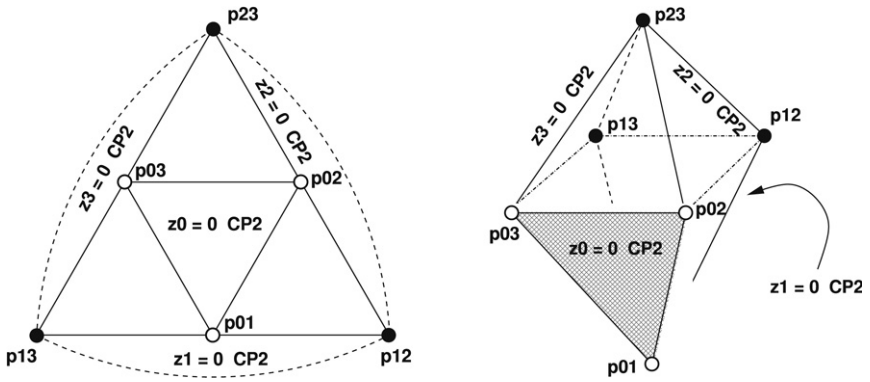

Fig. 11.

The n^3 triangles whose edges lie on three different $\mathbb{C}\mathbf{P}^2$'s, $z_1 = 0,\ z_2 = 0,\ z_3 = 0$, respectively, are:

$$\{p12_i,\ p13_j,\ p23_k\}, \quad i, j, k = 0, \ldots, n-1.$$

The rectangles can be divided into three groups: each of them has one edge lying on the $\mathbb{C}\mathbf{P}^2$ labeled by $z_0 = 0$ and an opposite edge on $z_m = 0,\ m = 1, 2, 3$. The group with $m = 1$, for example, contains the following n^3 rectangles:

$$\{p02_i,\ p03_j,\ p13_k,\ p12_l\}, \quad i - j + k - l = 0 \pmod{n}.$$

Fig. 12 is an actual image of a generic 4-cell using an explicit embedding of $\mathbb{C}\mathbf{P}^3$ into $\mathbb{R}^{16}$ (see, e.g., Hanson and Sha (2006)). (a) and (b) depict the 3-balls that are the upper and lower hemispheres of the S^3 bounding the 4-cell (see also Fig. 6). Note the distinct rectangles, which cut across the middle of the two 3-balls, dividing each into two pyramids; one pyramid in each 3-ball has been made transparent using wire-frame rendering to make the rectangle visible. (c) shows a complete partially transparent shaded rendering of the entire embedded 4-cell projected to 3D, with the outer octahedron being essentially the equator S^2 that is shared by the two hemispheres (a) and (b) of the S^3.

Finally, we briefly indicate how tessellation can help in computer graphics visualization of Fermat surfaces. We first embed the edges of a single 3-cell in $\mathbb{R}^{16}$ using our standard embedding of $\mathbb{C}\mathbf{P}^3$. The group Γ_n (which has order $24n^3$) acts transitively on the set of all the 3-cells with the isotropy group $\mathbb{Z}_2$ for the single 3-cell. Using computer algebra tools we produce a representative from each two-element equivalence class of $\Gamma_n/\mathbb{Z}_2$, and then we can generate all distinct $12n^3$ 3-cells. One also needs to choose appropriate projections to 3D to create the picture. This process becomes very complex even for F_4 (a K3 surface), which has 768 3-cells. With appropriate 3D projections, we can display various parts of F_4, and hence have a glance at its structure. Fig. 13 shows the chosen basic representative 3-cell; Fig. 14 presents four 3-cells generated from the representatives of $\Gamma_4/\mathbb{Z}_2$ that form the isotropy group, in Γ_4, of the quadrilateral base of the basic 3-cell. Fig. 15 shows the three sets of four rectangles sharing one edge of a fixed triangle; each vertex not on the triangle is shared by two of these rectangles, so 15 of the 24 vertices are generated in this way. Fig. 16 uses a projection that exposes all 24 vertices and draws schematic straight lines between them, with the shape of the basic 3-cell shown in heavy lines. Finally, Fig. 17 presents a similar projection of the correctly rendered edges for the entire K3 surface, giving a qualitative representation of a full tessellation based on our construction.

Further exploration of the properties of the family of tessellations we have presented requires more sophisticated interactive visualization tools to expose and examine the structures, e.g., by interactively selecting and reprojecting subsets of the tessellations in various ways to a 3D graphics environment.

Acknowledgements

Portions of the first author's work were supported by National Science Foundation Grants CCF-0204112 and IIS-0430730.

Please cite this article in press as: Hanson, A.J., Sha, J.-P., A tessellation for Fermat surfaces in $\mathbb{C}\mathbf{P}^3$. Journal of Symbolic Computation (2008), doi:10.1016/j.jsc.2008.09.002

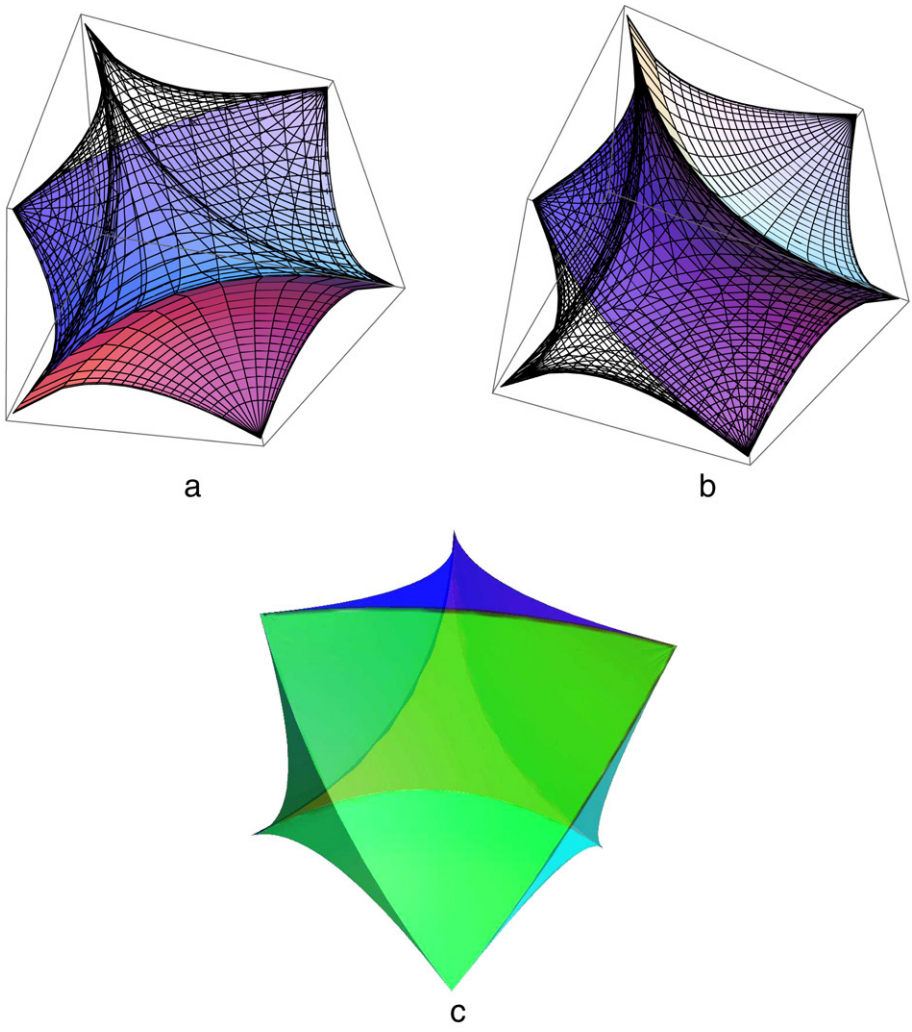

Fig. 12.

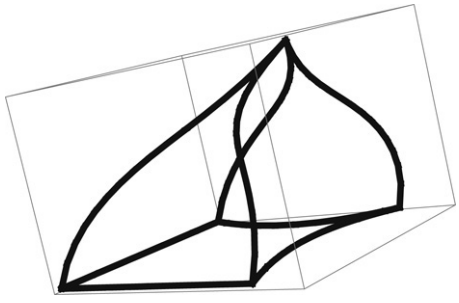

Fig. 13.

Please cite this article in press as: Hanson, A.J., Sha, J.-P., A tessellation for Fermat surfaces in $\mathbb{C}P^3$. Journal of Symbolic Computation (2008), doi:10.1016/j.jsc.2008.09.002

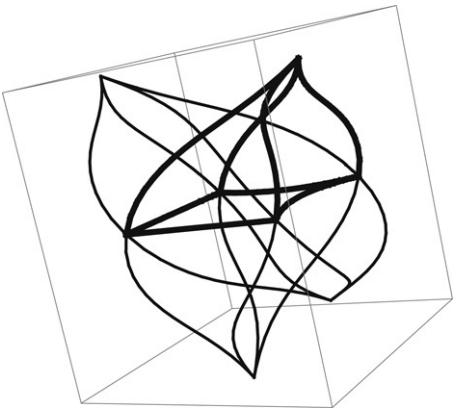

Fig. 14.

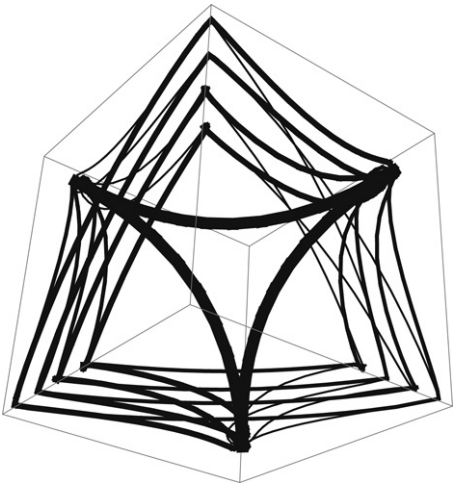

Fig. 15.

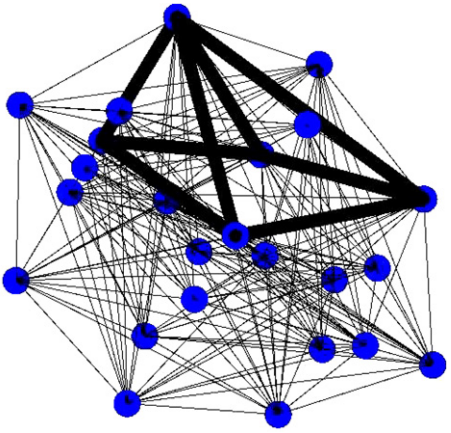

Fig. 16. The 24 vertices of the K3 tessellation.

Please cite this article in press as: Hanson, A.J., Sha, J.-P., A tessellation for Fermat surfaces in $\mathbb{C}P^3$. Journal of Symbolic Computation (2008), doi:10.1016/j.jsc.2008.09.002

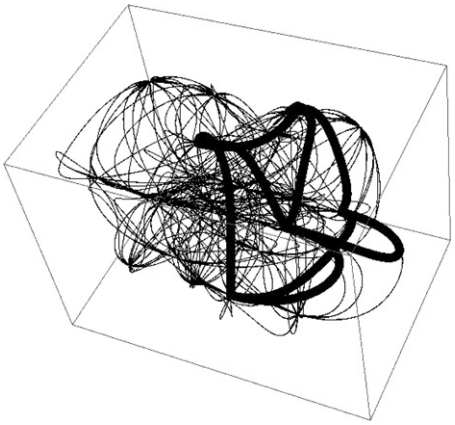

Fig. 17. The full K3 edges.

References

Greene, Brian, 1999. The Elegant Universe. Vintage, New York.
Griffiths, P., Harris, J., 1978. Principles of Algebraic Geometry. Wiley, New York.
Hanson, A.J., 1994. A Construction for computer visualization of certain complex curves. Notices of the American Mathematical Society 41 (9), 1156–1163.
Hanson, A.J., Sha, J.-P., 2006. A contour integral representation for the dual five-point function and a symmetry of the genus four surface in R^6. Journal of Physics A: Mathematics and General 39, 2509–2537.

Please cite this article in press as: Hanson, A.J., Sha, J.-P., A tessellation for Fermat surfaces in $\mathbb{C}P^3$. Journal of Symbolic Computation (2008), doi:10.1016/j.jsc.2008.09.002